

## Insight into the formation of bismuth-tungsten carbonyl clusters

Katrin Beuthert <sup>1,2</sup>, Benjamin Peerless<sup>1,2</sup> & Stefanie Dehnen <sup>1</sup>✉

Multimetallic clusters play a key role as models to doped metals, as candidates to new types of superatomic catalysts and as precursors to new multimetallic solids. Understanding formation pathways is an essential and necessary step forward in the development of cluster synthesis and research, yet remains considerably lacking owing to difficulty in identification of intermediates and the ill-defined nature of common starting materials. Here we show progress in this regard by investigating the reactivity of an intermetallic solid of nominal composition 'K<sub>5</sub>Ga<sub>2</sub>Bi<sub>4</sub>' with [W(cod)(CO)<sub>4</sub>] upon extraction with ethane-1,2-diamine (en) and 4,7,13,16,21,24-hexaoxa-1,10-diazabicyclo[8.8.8]hexacosane (crypt-222). Several polybismuthide intermediates and by-products were identified along the reaction pathway, ultimately forming the new polybismuthide salt [K(crypt-222)]<sub>3</sub>[μ<sub>3</sub>-Bi<sub>3</sub>{W(CO)<sub>3</sub>]<sub>2</sub>]•en•tol. DFT calculations revealed plausible reaction schemes for the transformations taking place in the reaction mixture providing insight into the complex reactivity of 'K<sub>5</sub>Ga<sub>2</sub>Bi<sub>4</sub>' on the basis of in situ generation of Bi<sub>2</sub><sup>2-</sup>.

<sup>1</sup>Karlsruhe Institute of Technology (KIT), Institute of Nanotechnology (INT), 76021 Karlsruhe, Germany. <sup>2</sup>These authors contributed equally: Katrin Beuthert, Benjamin Peerless. ✉email: [stefanie.dehnen@kit.edu](mailto:stefanie.dehnen@kit.edu)

Metal cluster molecules have been described as intermediary compounds between molecules and extended materials, or as model compounds for surface interactions involving the bulk phase especially when considering catalysis and their place in the “cluster-surface” analogy<sup>1–7</sup>. This is commonly employed with respect to transition metal carbonyl cluster compounds. Yet, despite their relevance and use, cluster molecules are in a position as exciting and fascinating compounds while their formation pathways are poorly understood. Given the vital role mechanistic detail applies to our greater knowledge of organic or organometallic chemistry, efforts to elucidate such pathways are essential<sup>8,9</sup>. The main drawback, in such efforts of cluster synthesis, is the limited understanding in how metal–metal bonds actually form in metal clusters, especially when there are several such bonds in a molecule. This lack of a retrosynthetic approach, ubiquitous in all fields of synthetic chemistry, significantly hinders this avenue of study. A starting point to solving these challenging problems lies in the diverse range of compounds that form upon the synthesis of a metal cluster compound. Zintl anions, homo- or heteroatomic anionic cluster molecules of the main group elements, are all-(semi)metal molecules with relatively flexible bonds, ideal as candidates for studying formation pathways in cluster synthesis<sup>10–12</sup>.

Intermetallic solid mixtures between alkali/alkaline earth metals and main group elements are the starting point for all known Zintl clusters<sup>13</sup>. Extraction of these mixtures with highly polar solvents, such as ethane-1,2-diamine (en) or liquid ammonia, in the presence of a sequestering agent, most commonly 4,7,13,16,21,24-hexaoxa-1,10-diazabicyclo[8.8.8]hexacosane (crypt-222), yields homoatomic or heteroatomic Zintl anions depending on the solid mixture used. When another reagent is added to the solid mixture, such as a transition metal (or f-block metal) complex, the Zintl anion can then be modified or expanded<sup>14</sup>. Realization of this reactivity opens up an incredible wealth of possibilities. The choice of transition metal and ligand sphere of the complex can have a profound effect on the outcome of the final product, as well as on the properties of the new cluster itself<sup>15</sup>. The functionalization and reactivity of Zintl clusters have been reviewed numerous times, and several new endeavours since these reviews, highlighting enhanced solubilization and catalysis for example, have been made<sup>11,13–20</sup>. What is becoming clear is that Zintl clusters—both naked and functionalised—are moving away from academic curiosities toward functional compounds in their own right<sup>19,21–24</sup>. With this, addressing the challenge of the formation pathways of these structurally complex and beautiful molecules is more apparent. This also addresses the efficiency of cluster formation or prediction. There are a few studies highlighting such pathways, and notably how difficult it is to model and predict the processes involved<sup>10,12,25–27</sup>.

Therefore, we wanted to investigate cluster formation pathways in a systematic manner. The reactions between transition metal carbonyl clusters and Bi-based Zintl anions have been investigated a number of times in terms of the identification of products, but little insight into their formation. Seemingly, transition metal carbonyl complex fragments as a part of polybismuthide–metal cluster molecules,  $[\text{Bi}_x\{\text{M}(\text{CO})_y\}_z]^{q-}$ , that can be described as having fewer than 12 electrons, like  $[\text{M}(\text{CO})]^{+}$  ( $\text{M} = \text{Co}, \text{Rh}, \text{Ir}$ ) with 10 electrons, yield cluster motifs typical for electron-rich species (thus, not consistent with deltahedral cage types)<sup>28–30</sup>. In contrast, those with 12 electrons,  $[\text{Ni}(\text{CO})]$ ,  $[\text{Cr}(\text{CO})_3]$  and  $[\text{Mo}(\text{CO})_3]$  for example, do typically possess deltahedral (*closo*-) structures, as typical for electron-deficient cages<sup>31–36</sup>. Selected examples of known polybismuthide–metal clusters with CO ligands are shown in Fig. 1.

Another factor in the various structures observed is the flexibility of polybismuthide substructures where the  $\{\text{Bi}_n\}$  fragment

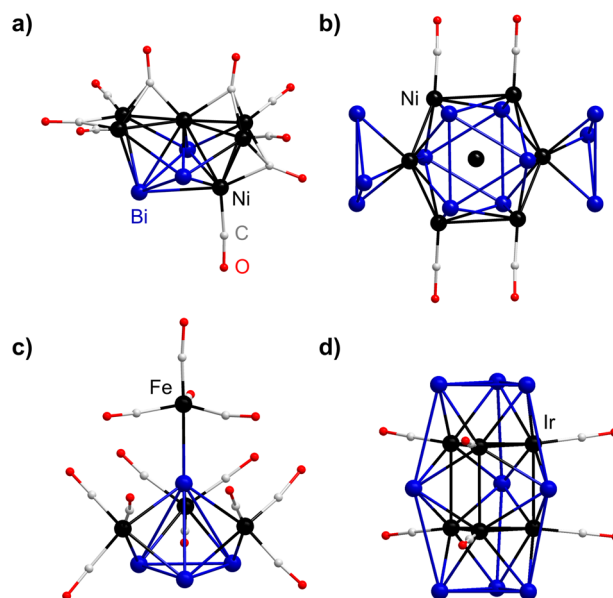


**Fig. 1** Examples of structures of known polybismuthide–metal clusters bearing CO ligands. **a**  $[\text{Bi}_3\text{Ni}_6(\text{CO})_9]^{3-}$ <sup>32</sup>. **b**  $[\text{Ni}@\{\text{Bi}_6\text{Ni}_6(\text{CO})_8\}]^{4-}$ <sup>32</sup>. **c**  $[\text{Bi}_4\text{Fe}_4(\text{CO})_{13}]^{2-}$ <sup>31</sup>. **d**  $[(\eta^3\text{-Bi}_3)_2(\text{IrCO})_6(\mu^4\text{-Bi})_3]^{2-}$ <sup>29</sup>.

can range with values of  $n = 1–6$  forming chains, rings, butterfly structures and even prisms and crowns. With such versatility in both the polybismuthide and transition metal complex fragment possible, insight into their formation would provide extensive information into cluster formation in general and even the potential of cluster design and fabrication on demand. Here, we report on the reactivity of a Bi intermetallic solid mixture, as a source for Bi-based Zintl anions, with group 6 transition metal carbonyl complexes. By isolation of several intermediate and by-product compounds along the reaction path accompanied by comprehensive quantum chemical studies, we have devised a pathway for the formation of complex polybismuthide–transition metal carbonyl clusters in an effort to elucidate key processes which can occur during cluster formation.

## Results and discussion

**Synthesis and structures.** The intermetallic solid with the nominal composition “ $\text{K}_5\text{Ga}_2\text{Bi}_4$ ” has been used successfully multiple times as a source of polybismuthides and Bi-based Zintl clusters<sup>10,37–41</sup>. It has been suggested that the negatively charged Ga atoms in this mixture can act as a source of electrons by the release of elemental Ga to afford polybismuthides in the reaction mixture. This includes those that have not, or cannot, be isolated themselves, like  $\text{Bi}_3^{9-}$ , which has been observed in mass spectrometric measurements and long been postulated as an intermediate towards larger polybismuthides. To date, the only Ga- and Bi-containing anionic clusters reported are  $(\text{GaBi}_3)^{2-}$  (see ref. 41),  $(\text{Ga}_2\text{Bi}_6)^{4-}$ ,  $[\text{Bi}@\text{Ga}_8(\text{Bi}_2)_6]^{q-}$  ( $q = 3$  or  $5$ )<sup>10</sup> and  $[\text{Sm}@\text{Ga}_2\text{HBi}_{11}]^{3-}$  (see ref. 40), with only the former being discussed to form upon extraction of the intermetallic solid alone; the other clusters requiring an oxidizing agent added during the extraction process, as their overall negative charge per atom is lower than that in the precursor material. Nevertheless, with several uncertainties it is clear the reactivity of “ $\text{K}_5\text{Ga}_2\text{Bi}_4$ ” is complex and requires further investigation given the effective application of this solid in Zintl cluster syntheses. We have therefore undertaken a systematic study into cluster formation reactions using “ $\text{K}_5\text{Ga}_2\text{Bi}_4$ ” and one selected transition metal complex. On the combination of a 1:1.5 mixture of “ $\text{K}_5\text{Ga}_2\text{Bi}_4$ ”,  $[\text{W}(\text{cod})(\text{CO})_4]$  ( $\text{cod} = 1,5\text{-cyclooctadiene}$ ) and crypt-222 in en, a

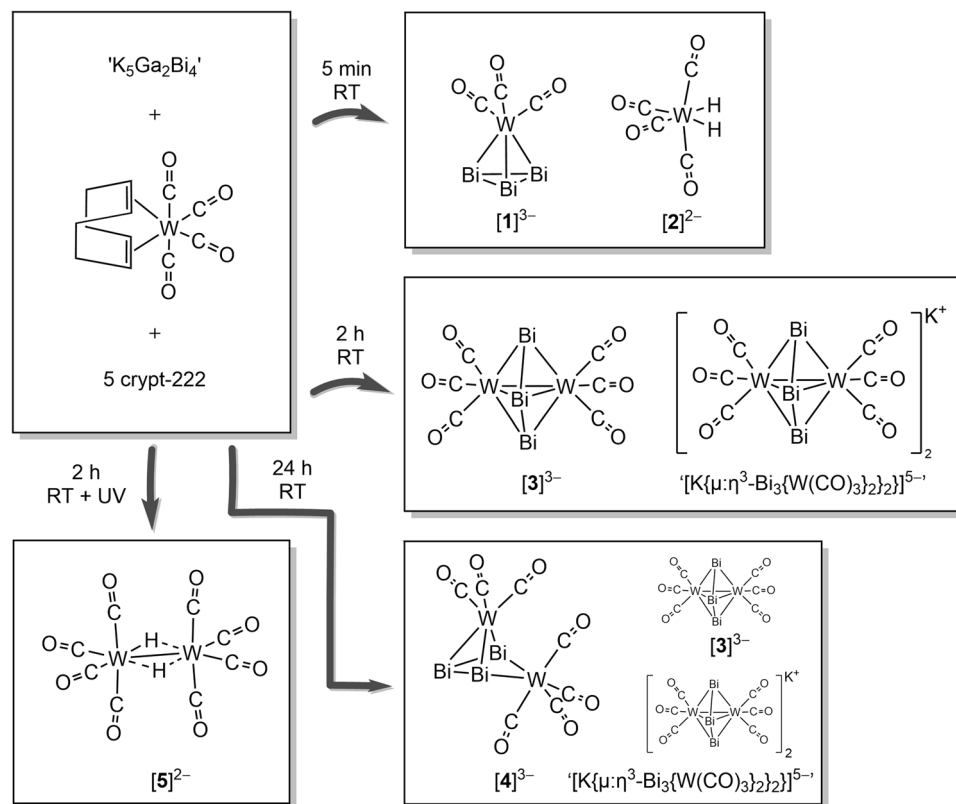


**Fig. 2** Sequential formation of the cluster compounds and complexes discussed in this work. The starting materials are shown in the top left corner, with all subsequent steps indicated by arrows.

dark green suspension forms. Depending on the time which the suspension is allowed to stir different products are obtained. The reaction was effectively stopped by filtering the supernatant solution off the reactive intermetallic solid and subsequently layering it with toluene for crystallization (see experimental section for more detailed description). All isolated crystals' constitution was additionally confirmed by micro-X-ray fluorescence spectroscopy ( $\mu$ -XFS). Efforts to obtain more in situ data by optical spectroscopy or mass spectrometry was unsuccessful, therefore the following results are a combination of structural data and in-depth quantum chemical calculations.

After a reaction time of five minutes, crystals of two habits had formed: black, block crystals and green, plate crystals. Photographs of single crystals and reaction solutions are shown in Supplementary Fig. 1. The crystals were identified as  $[K(\text{crypt-222})]_3[\eta^3\text{-Bi}_3\text{W}(\text{CO})_3]\cdot 3\text{en}\cdot 3\text{tol}$  ( $[K(\text{crypt-222})]_3\mathbf{1}\cdot 3\text{en}\cdot 3\text{tol}$ ) and  $[K(\text{crypt-222})]_2[\text{W}(\text{CO})_4(\text{H})_2]\cdot \text{en}$  ( $[K(\text{crypt-222})]_2\mathbf{2}\cdot \text{en}$ ) by single-crystal X-ray diffraction, respectively. When the reaction time was prolonged to two hours, neither  $[K(\text{crypt-222})]_3\mathbf{1}\cdot 3\text{en}\cdot 3\text{tol}$  or  $[K(\text{crypt-222})]_2\mathbf{2}\cdot \text{en}$  was observed. In fact, two new compounds crystallized instead,  $[K(\text{crypt-222})]_3[\mu:\eta^3\text{-Bi}_3\{\text{W}(\text{CO})_3\}_2]\cdot \text{en}\cdot \text{tol}$  ( $[K(\text{crypt-222})]_3\mathbf{3}\cdot \text{en}\cdot \text{tol}$ ) and  $[K(\text{crypt-222})]_5[K\{\mu:\eta^3\text{-Bi}_3\{\text{W}(\text{CO})_3\}_2\}_2]\cdot 2\text{en}$  as black needle and dark red needle crystals, respectively. Both  $[K(\text{crypt-222})]_3\mathbf{3}\cdot \text{en}\cdot \text{tol}$  and  $[K(\text{crypt-222})]_5[K\{\mu:\eta^3\text{-Bi}_3\{\text{W}(\text{CO})_3\}_2\}_2]\cdot 2\text{en}$  contain the same  $[\mu:\eta^3\text{-Bi}_3\{\text{W}(\text{CO})_3\}_2]^{3-}$  unit, which can be viewed as an addition of a  $\{\text{W}(\text{CO})_3\}$  fragment to anion  $[1]^{3-}$ , though evidence suggests that it is more likely that these two compounds form upon addition of a  $\{\text{W}(\text{CO})_4\}$  unit to anion  $[1]^{3-}$  first. Upon increasing the reaction time to 24 h,  $[K(\text{crypt-222})]_3\mathbf{3}\cdot \text{en}\cdot \text{tol}$  and  $[K(\text{crypt-222})]_5[K\{\mu:\eta^3\text{-Bi}_3\{\text{W}(\text{CO})_3\}_2\}_2]\cdot 2\text{en}$  again crystallize from the solution, however, a third compound also crystallizes alongside,  $[K(\text{crypt-222})]_3[\mu^2:\eta^3\text{-Bi}_3\{\text{W}(\text{CO})_3\text{W}(\text{CO})_4\}]\cdot 3\text{en}\cdot \text{tol}$  ( $[K(\text{crypt-222})]_3\mathbf{4}\cdot 3\text{en}\cdot \text{tol}$ ), as black, block crystals. One additional experiment performed was the exposure of the reaction mixture to UV-A radiation. No bismuth-containing product was obtained, only  $[K(\text{crypt})]_2[\text{W}_2\text{CO}_8(\mu\text{-H}_2)]\cdot 0.5\text{tol}$  ( $[K(\text{crypt-222})]_2\mathbf{5}\cdot 0.5\text{tol}$ ) was observed from a dark-brown solution as yellow plate-shaped crystals. Mass spectrometric measurements of reaction solutions and samples made from isolated crystals were unsuccessful. The observations made after different reaction times are summarized in Fig. 2.

222)]<sub>3</sub>4·3en·tol), as black, block crystals. One additional experiment performed was the exposure of the reaction mixture to UV-A radiation. No bismuth-containing product was obtained, only  $[K(\text{crypt})]_2[\text{W}_2\text{CO}_8(\mu\text{-H}_2)]\cdot 0.5\text{tol}$  ( $[K(\text{crypt-222})]_2\mathbf{5}\cdot 0.5\text{tol}$ ) was observed from a dark-brown solution as yellow plate-shaped crystals. Mass spectrometric measurements of reaction solutions and samples made from isolated crystals were unsuccessful. The observations made after different reaction times are summarized in Fig. 2.

All six products were characterized by single-crystal X-ray crystallography. Crystallographic details are provided in Supplementary Data 1–5. Compounds  $[K(\text{crypt-222})]_3\mathbf{1}\cdot 3\text{en}\cdot 3\text{tol}$  and  $[K(\text{crypt-222})]_5[K\{\mu:\eta^3\text{-Bi}_3\{\text{W}(\text{CO})_3\}_2\}_2]\cdot 2\text{en}$  are the W analogs of previously described compounds of the lighter congeners Cr and Mo<sup>36,42</sup>, and due to disorder and poor data quality will not be discussed in detail beyond their connectivity.  $[1]^{3-}$  has a three-legged piano stool structure with a  $\{\text{Bi}_3\}$  triangle capping the top, consistent with the previously reported structures containing Cr and Mo. The anion  $[K\{\mu:\eta^3\text{-Bi}_3\{\text{W}(\text{CO})_3\}_2\}_2]^{5-}$  has the same structure as the anion in  $[K(\text{crypt-222})]_5[K\{\text{Bi}_3\text{M}_2(\text{CO})_6\}_2]$  ( $\text{M} = \text{Cr}$  and  $\text{Mo}$ )<sup>36</sup>, it is given here in inverted commas, as the data sets collected from the crystals did not allow for a proper refinement of the entire crystal structure, although it can be assumed to be homologous to the lighter homolog. Compounds  $[K(\text{crypt-222})]_2\mathbf{2}\cdot \text{en}$ ,  $[K(\text{crypt-222})]_3\mathbf{3}\cdot \text{en}\cdot \text{tol}$ ,  $[K(\text{crypt-222})]_3\mathbf{4}\cdot 3\text{en}\cdot \text{tol}$  and  $[K(\text{crypt-222})]_2\mathbf{5}\cdot 0.5\text{tol}$  are all newly identified structures. Anion  $[3]^{3-}$  has the same  $\mu^3$ -“ozone-like”  $\{\text{Bi}_3\}$  structure bridging between two  $\{\text{W}(\text{CO})_3\}$  fragments observed in the structures of the  $[K(\text{crypt-222})]_5[K\{\text{Bi}_3\text{M}_2(\text{CO})_6\}_2]$  series ( $\text{M} = \text{Cr}$ ,  $\text{Mo}$ ,  $\text{W}$ ). The Bi–Bi bond lengths of the  $\{\text{Bi}_3\}$  are slightly longer in the W case (3.015(1)/3.016(1) Å vs 2.956/2.954 for Cr vs 2.987/2.987 for Mo), and consistent with a bond length larger than a Bi=Bi double bond. In addition, the W–Bi bond lengths are also slightly

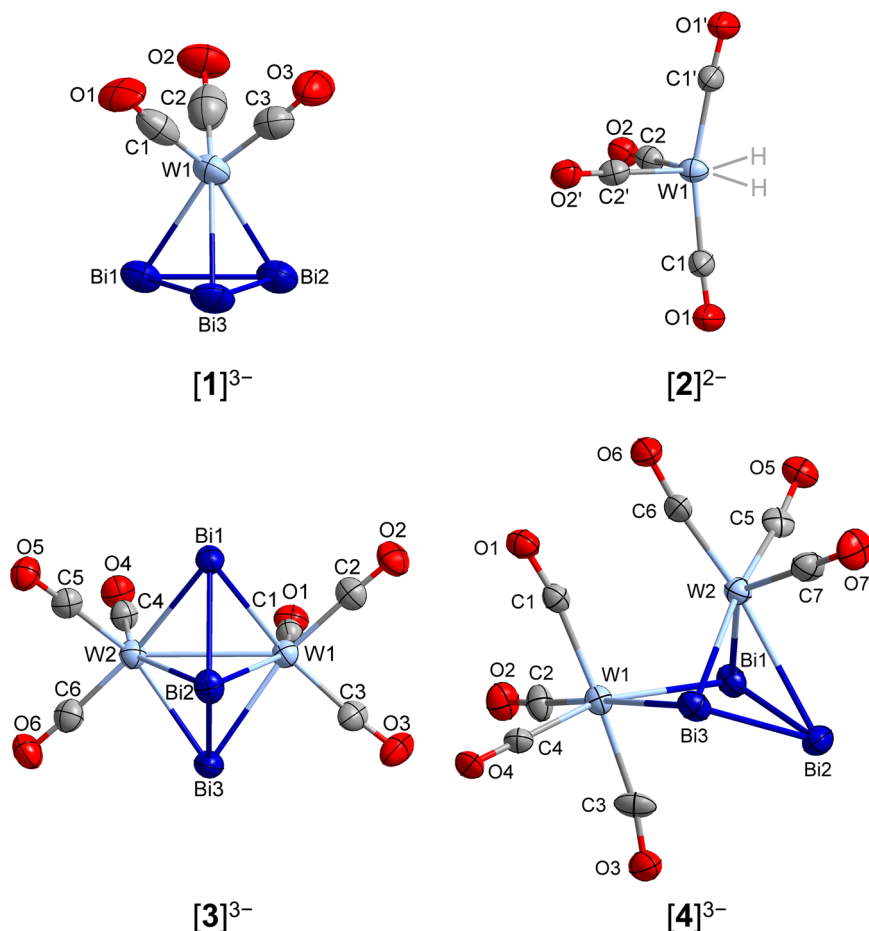


**Fig. 3** Molecular structures of the anions  $[\eta^3\text{-Bi}_3\text{W}(\text{CO})_3]^{3-}$  ( $[1]^{3-}$ ),  $[\text{W}(\text{CO})_4(\text{H})_2]^{2-}$  ( $[2]^{2-}$ ),  $[\mu\text{-}\eta^3\text{-Bi}_3\{\text{W}(\text{CO})_3\}_2]^{3-}$  ( $[3]^{3-}$ ), and  $[\mu^2\text{-}\eta^3\text{-Bi}_3\{\text{W}(\text{CO})_3\text{W}(\text{CO})_4\}]^{3-}$  ( $[4]^{3-}$ ). The structures were determined by means of single-crystal X-ray diffraction of the corresponding salts. Note that the H atoms in  $[2]^{2-}$  could not be refined from the difference Fourier map, nor could they be affixed to the structure; their positions are therefore indicated schematically. However, the presence of H atoms at these coordination sites was unambiguously confirmed by quantum chemical calculations of the structure of the  $\{\text{W}(\text{CO})_4\}^{2-}$  fragment with and without the H atoms (see below).

longer compared to the Cr and Mo examples, as expected for the larger metal atom, and follow the same trend that the  $\text{W}-\text{Bi}_{(\text{BiBiBi})}$  bond lengths (2.831(1)-2.860(1) Å) are shorter than  $\text{W}-\text{Bi}_{(\text{BiBiBi})}$  (3.115(1)-3.120(1) Å). The presence of this  $\{\text{Bi}_3\}$  moiety locks the geometry about the W atoms in place, forcing the three CO ligands on each metal atom into an eclipsed conformation. Anion  $[4]^{3-}$  is an interesting extension to the coordination chemistry of  $\{\text{Bi}_3\}$  fragments. In the molecular structure, the  $\{\text{Bi}_3\}$  unit does not bridge symmetrically between the two chemically different W atoms. One W atom, that belongs to the  $\{\text{W}(\text{CO})_3\}$  fragment, is bonded to the three Bi atoms in an  $\eta^3$ -fashion whilst the W atom of the  $\{\text{W}(\text{CO})_4\}$  fragment is only bonded to two of the Bi atoms affording six bonds to each W atom. This  $\eta^2$ -coordination, in fact, effectively forms a puckered four-membered  $\{\text{WBi}_3\}$  ring, which coordinates through the three Bi atoms to  $\{\text{W}(\text{CO})_3\}$  giving a geometry consistent with a three-legged piano stool complex for this W atom. A result of the different coordination mode in  $\{\text{W}_2\text{Bi}_3\}$  leads to a slight decrease in the Bi–Bi bond length (2.961(1) and 2.987(1) Å) and a narrower Bi–Bi–Bi bond angle (90.34(3)° vs. 96.26(2)°) compared to that of anion  $[3]^{3-}$ . The  $\{(\text{CO})_4\text{W}\}-\text{Bi}$  bond lengths are similar to one another (2.968(1) and 2.994(1) Å) yet slightly longer than  $\{(\text{CO})_3\text{W}\}-\mu\text{Bi}$  (2.839(1) and 2.883(1) Å), the other  $\{(\text{CO})_3\text{W}\}-\text{Bi}$  bond length is the longest in the molecule (3.077(1) Å). Three of the CO ligands in the  $\{\text{W}(\text{CO})_4\}$  fragment are in an eclipsed arrangement with

respect to the CO ligands of the  $\{\text{W}(\text{CO})_3\}$  fragment, and the fourth CO of the  $\{\text{W}(\text{CO})_4\}$  lies in the same plane as the non-bridging Bi atom. The molecular structures of the products are shown in Fig. 3.

At first glance, it can be thought that  $[4]^{3-}$  is the product of a reaction between  $[1]^{3-}$  and  $[\text{W}(\text{cod})(\text{CO})_4]$  starting material with concurrent loss of cod ligand. However, it then appears that the last compound to be experimentally observed is a compound that should be consumed at an earlier stage, as it is feasible that  $[3]^{3-}$  and “ $[\text{K}\{\mu\text{-}\eta^3\text{-Bi}_3\{\text{W}(\text{CO})_3\}_2\}]^{5-}$ ” could be generated by loss of CO from  $[4]^{3-}$ . This idea is further supported that after allowing the mixture to stir for 48 h only  $[\text{K}(\text{crypt-222})_3\text{3-en-tol}]$  was isolated, additionally by stirring the mixture for 2 h at 60 °C the same outcome was observed. Though there is no quantitative kinetic evidence, only a qualitative description can be formed, suggesting that both the formation of the anionic complexes  $[3]^{3-}$  and  $[4]^{3-}$  are similarly slow processes. As mentioned above, irradiation by light did not yield another Bi-based compound, but led to the formation of the dinuclear W complex  $[5]^{2-}$ .

**Quantum chemical calculations and formation pathway.** To provide further insight into the reaction cascade, DFT calculations on all anionic molecules were performed, using the TURBO-MOLE program suite<sup>43</sup>. We employed the TPSS functional<sup>44</sup> and dhf-TZVP basis sets<sup>45</sup> including pseudo potentials ECP-60 for W



222)]<sub>2</sub>·5·0.5tol is made up of two {W(CO)<sub>4</sub>} fragments, which are correspondingly bridged by two hydrogen atoms, leading to octahedral geometries about both W atoms again. The W···W distance is 3.021(1) Å. Similarly to [2]<sup>2-</sup>, the W–C bond lengths of the *trans*-CO ligands are slightly longer than the *cis*-CO ligands (1.978(8) and 1.929(8) Å). Unlike in [2]<sup>2-</sup>, the C–W–C ligands are consistent with a rather perfectly octahedral geometry of approximately 90 and 180°. It is reasonable to assume that [5]<sup>2-</sup> is formed by the oxidative coupling of two [2]<sup>2-</sup> upon release of H<sub>2</sub> initiated by UV-light.

To summarize, several compounds which represent snapshots along the reaction pathway from the reaction between “K<sub>5</sub>Ga<sub>2</sub>Bi<sub>4</sub>” and [W(cod)(CO)<sub>4</sub>] in en have been identified, with the final product being the salt of the [μ<sub>3</sub>-Bi<sub>3</sub>{W(CO)<sub>3</sub>}<sub>2</sub>]<sup>3-</sup> anion. From our observations, and supported by DFT calculations, balanced reaction schemes have been described for these processes which has shed light onto the reactivity of “K<sub>5</sub>Ga<sub>2</sub>Bi<sub>4</sub>” for the first time in such detail. The still ill-defined intermetallic solid has been proven as a source for a variety of polybismuthides or (GaBi<sub>3</sub>)<sup>2-</sup>, however, according to our findings, it is Bi<sub>2</sub><sup>2-</sup> that fits best as the reactive component of the extracted solution. The versatility of this simple molecule provides an excellent starting point for the growth of polybismuthide structures. With every study, the understanding and prediction of polybismuthide synthesis is becoming easier yet we are still only scratching the surface into the vast potential of these compounds.

## Methods

**General methods.** All syntheses were performed under the exclusion of air and moisture using standard Schlenk or glovebox techniques. Ethane-1,2-diamine (en) was distilled from CaH<sub>2</sub> and stored over 3 Å molecular sieves. Toluene (tol, Acros Organics, 99%) was distilled from sodium and stored over 3 Å molecular sieves. Kryptofix® 222 (crypt-222, Sigma Aldrich) was dried under vacuum for at least 18 h. [W(cod)(CO)<sub>4</sub>] was purchased from Sigma Aldrich. “K<sub>5</sub>Ga<sub>2</sub>Bi<sub>4</sub>” was prepared by stoichiometric fusion of the elements at 600 °C for 7 days in a niobium tube, sealed within an evacuated silica ampoule. For the standard procedure, “K<sub>5</sub>Ga<sub>2</sub>Bi<sub>4</sub>” (0.1 g, 85.4 μmol), [W(cod)(CO)<sub>4</sub>] (0.037 g, 85.4 μmol, 1 eq), and crypt-222 (0.161 g, 431.1 μmol, 5 eq) were dissolved in 4 ml en in a Schlenk tube and stirred at room temperature for a certain amount of time. Photographs of as-prepared crystal are shown in Supplementary Fig. 1.

**Synthesis of ([K(crypt-222)]<sub>3</sub>1·3en·3tol and ([K(crypt-222)]<sub>2</sub>2·en.** Following the standard procedure, the dark green reaction solution was filtered through a glass frit after five minutes. The dark green filtrate was layered with 5 ml tol for crystallization. After 1 week black, block crystals of ([K(crypt-222)]<sub>3</sub>1·3en·3tol and green plate crystals of ([K(crypt-222)]<sub>2</sub>2·en had formed.

**Synthesis of ([K(crypt-222)]<sub>3</sub>3·en·tol and “[K(crypt-222)]<sub>5</sub>[K{μ<sub>3</sub>-Bi<sub>3</sub>{W(CO)<sub>3</sub>}<sub>2</sub>}]·2en”.** By extending the reaction time of the standard procedure to 2 h, no change in the color of the reaction solution was observed. The dark green reaction solution was layered with 5 ml tol. After 3 days, dark red needle crystals of ([K(crypt-222)]<sub>3</sub>3·en·tol and after one week black needle crystals of “[K(crypt-222)]<sub>5</sub>[K{μ<sub>3</sub>-Bi<sub>3</sub>{W(CO)<sub>3</sub>}<sub>2</sub>}]·2en” had formed. The reaction could be repeated at 60 °C with the same results.

**Synthesis of ([K(crypt-222)]<sub>3</sub>4·3en·tol.** The standard procedure was carried out with a reaction time of 24 h. The dark green reaction solution was filtered through a glass frit and layered with 5 ml tol. After 3 days, crystals in the form of black blocks, identified as ([K(crypt-222)]<sub>3</sub>4·3en·tol were obtained, beside crystals of [K(crypt-222)]<sub>3</sub>3·en·tol, and after one week also crystals of “[K(crypt-222)]<sub>5</sub>[K{μ<sub>3</sub>-Bi<sub>3</sub>{W(CO)<sub>3</sub>}<sub>2</sub>}]·2en”.

**Synthesis of [K(crypt-222)]<sub>5</sub>·0.5tol.** “K<sub>5</sub>Ga<sub>2</sub>Bi<sub>4</sub>” (0.1 g, 85.4 μmol), [W(cod)(CO)<sub>4</sub>] (0.037 g, 85.4 μmol, 1 eq), and crypt-222 (0.161 g, 431.1 μmol, 5 eq) were dissolved in 4 ml en in a Schlenk tube and stirred for 2 h at room temperature and irradiated with UV-A light by application of an ULTRA-VITALUX UV-A lamp (Osram). The dark-brown solution was filtered using a glass frit. The brown filtrate was layered with 5 ml of tol. After 2 days, golden yellow crystals of [K(crypt-222)]<sub>5</sub>·0.5tol were obtained in the form of thin platelets, additionally black cubes could be obtained. The structure of the cubes could not be analyzed.

**Micro-X-ray fluorescence spectroscopy (μ-XFS).** All μ-XFS measurements were performed on single-crystal samples with a Bruker M4 Tornado, equipped with an Rh-target X-ray tube, poly capillary optics and a Si drift detector. The emitted fluorescence photons are detected with an acquisition time of 180 s. Quantification of the elements is achieved through deconvolution of the spectra. Results are shown in Supplementary Table 1 and Supplementary Figs. 2–6, and it should be noted that for samples of Zintl cluster salts, the determination of the K content typically shows some deviations.

**Electrospray ionization mass spectrometry (ESI-MS).** ESI mass spectra were recorded with a Thermo Fischer Scientific Finnigan LTQ-FT spectrometer in the negative ion mode. In situ samples were taken from the reaction mixture and used directly. The solutions were injected into the spectrometer with gastight 250 μL Hamilton syringes by syringe pump infusion. All capillaries within the system were washed with dry en 2 h before and at least 5 min in between measurements to avoid decomposition reactions and consequent clogging. The following ESI parameters were used: Spray Voltage: 3.6 kV, Capillary Temp: 290 °C, Capillary Voltage: –20 kV, Tube lens Voltage: –121.75 kV, Sheath Gas: 45, Sweep Gas: 0, Auxiliary Gas: 40. The overview spectrum is given in Supplementary Fig. 7. Assignable signals are summarized in Supplementary Table 2, with the corresponding high-resolution spectra shown in Supplementary Figs. 8–12.

**Single-crystal X-ray diffraction data.** The data for the X-ray structural analyses were collected at T = 100.0 K with Mo-Kα-radiation (λ = 0.71073 Å) on area detector systems Stoe IPDS/2T for X, Y, and Z and with Cu-Kα-radiation (λ = 1.54186 Å) for X, Y, Z on an area detector system Stoe StadiVari. The structures were solved by methods of SHELXT from SHELXL-2018/136, and refined by full-matrix least-squares methods against I<sup>2</sup> with the SHELXL<sup>52</sup> program using Olex2 v1.3.0 software<sup>53</sup>. All hydrogen atoms were kept riding on calculated positions with isotropic displacement parameters U = 1.2 U<sub>eq</sub> of the bonding partners. The crystal data and experimental parameters of the structure determination are collected in Supplementary Tables 3–8. Supplementary structural images are shown in Supplementary Figs. 13–26. Figures were created with Diamond 4<sup>54</sup>.

**Infrared (IR) spectroscopy.** The sample was measured as solid on a BRUKER Alpha-P ATR-FT-IR spectrometer with a diamond ATR probe head in an inert gas atmosphere. The spectra were evaluated using the program OPUS 6.5. The position of the absorption bands is given in wavenumbers ν (unit cm<sup>-1</sup>). Measurements were made in the range 4000–500 cm<sup>-1</sup>. The experimental spectrum is given in Supplementary Fig. 27, and calculated IR spectra are shown in Supplementary Figs. 28–32.

**Quantum chemical calculations.** DFT calculations were done with the program system TURBOMOLE<sup>43</sup> using the TPSS functional<sup>44</sup> and employing dhf-TZVP basis sets<sup>45</sup>, for Bi and W, Dirac-Fock in combination with effective core potentials ECP-60<sup>46</sup>. The conductor-like screening model (COSMO; ε = infinity, rsolv = 1.3) was used for charge compensation of the anionic molecules<sup>47</sup>. Localized molecular orbitals were obtained according to Boys' method<sup>55</sup>. The geometric and electronic structures were optimized simultaneously; resulting molecular structures are summarized in Supplementary Table 9. Additional reaction steps and corresponding reaction energies are given in Supplementary Figs. 33 and 34.

## Data availability

All data generated or analyzed during this study are included in this published article and its supplementary information files. The structures of compounds [K(crypt-222)]<sub>5</sub>[η<sup>3</sup>-Bi<sub>3</sub>W(CO)<sub>3</sub>]-3en·3tol ([K(crypt-222)]<sub>3</sub>1·3en·3tol), [K(crypt-222)]<sub>2</sub>[W(CO)<sub>4</sub>(H)<sub>2</sub>]-en ([K(crypt-222)]<sub>2</sub>2·en), [K(crypt-222)]<sub>3</sub>[μ<sub>3</sub>-Bi<sub>3</sub>{W(CO)<sub>3</sub>}<sub>2</sub>]-en·tol ([K(crypt-222)]<sub>3</sub>3·en·tol), [K(crypt-222)]<sub>3</sub>[μ<sup>2</sup>-η<sup>3</sup>-Bi<sub>3</sub>{W(CO)<sub>3</sub>W(CO)<sub>4</sub>}]·3en·tol ([K(crypt-222)]<sub>3</sub>4·3en·tol), and [K(crypt-222)]<sub>5</sub>[W<sub>2</sub>CO<sub>8</sub>(μ-H<sub>2</sub>)]·0.5tol ([K(crypt-222)]<sub>5</sub>·0.5tol) were determined by single-crystal X-ray diffraction. The X-ray crystallographic coordinates for structures reported in this Article have been deposited at the Cambridge Crystallographic Data Centre (CCDC), under deposition numbers CCDC-2239217 ([K(crypt-222)]<sub>3</sub>1·3en·3tol), CCDC-2239218 ([K(crypt-222)]<sub>2</sub>2·en), CCDC-2239219 ([K(crypt-222)]<sub>3</sub>3·en·tol), CCDC-2239220 ([K(crypt-222)]<sub>3</sub>4·3en·tol), and CCDC-2239221 ([K(crypt-222)]<sub>5</sub>·0.5tol). These data can be obtained free of charge from The Cambridge Crystallographic Data Centre via [www.ccdc.cam.ac.uk/data\\_request/cif](http://www.ccdc.cam.ac.uk/data_request/cif). The information is also provided as Supplementary Data 1–5 (CIF format). The Cartesian coordinates of all optimized structures and the respective SCF energies are summarized in Supplementary Data 6 (ASCII format). The files comprise all the necessary data for reproducing the values.

## Code availability

The TURBOMOLE quantum program suite is available from <https://www.turbomole.org> (retrieved January 27, 2023).

Received: 2 February 2023; Accepted: 17 May 2023;

Published online: 05 June 2023

## References

- Martino, G. *Clusters: Models and precursors for metallic catalysts. Growth and Properties of Metal Clusters*. (Elsevier, 1979).
- Laine, R. M. Criteria for identifying transition metal cluster-catalyzed reactions. *J. Mol. Catal.* **14**, 137–169 (1982).
- Braunstein, P. & Rose, J. *Heterometallic Clusters for Heterogeneous Catalysis* (Wiley-VCH, 1998).
- Rosenberg, E. & Laine, R. *Concepts and Models for Characterizing Homogeneous Reactions Catalyzed by Transition Metal Clusters* (Wiley-VCH, 1998).
- Jongh, L. J. Physical properties of metal cluster compounds. *Model Systems for Nanosized Metal Particles*. (eds. Braunstein, P., Oro, L. A. & Raithby, P. R.) 1434–1453 (Wiley-VCH, 1999).
- Sharapa, D. I., Doronkin, D. E., Studt, F., Grunwaldt, J. D. & Behrens, S. Moving frontiers in transition metal catalysis: synthesis, characterization and modeling. *Adv. Mater.* **31**, 1807381 (2019).
- Nielsen, M. T., Padilla, R. & Nielsen, M. Homogeneous catalysis by organometallic polynuclear clusters. *J. Clust. Sci.* **31**, 11–61 (2020).
- Davey, S. G. Retrosynthesis: computer says yes. *Nat. Rev. Chem.* **2**, 1 (2018).
- Talanquer, V. Importance of understanding fundamental chemical mechanisms. *J. Chem. Educ.* **95**, 1905–1911 (2018).
- Pan, F. et al. Insights into formation and relationship of multimetallic clusters: on the way toward bi-rich nanostructures. *J. Am. Chem. Soc.* **143**, 7176–7188 (2021).
- Weinert, B., Mitzinger, S. & Dehnen, S. (Multi-)metallic cluster growth. *Chem. Eur. J.* **24**, 8470–8490 (2018).
- Mitzinger, S., Broeckert, L., Massa, W., Weigend, F. & Dehnen, S. Understanding of multimetallic cluster growth. *Nat. Commun.* **7**, 10480 (2016).
- Scharfe, S., Kraus, F., Stegmaier, S., Schier, A. & Fässler, T. F. Zintl ions, cage compounds, and intermetallic clusters of group 14 and group 15 elements. *Angew. Chem. Int. Ed.* **50**, 3630–3670 (2011).
- Wilson, R. J., Lichtenberger, N., Weinert, B. & Dehnen, S. Intermetallic and heterometallic clusters combining p-block (semi)metals with d- or f-block metals. *Chem. Rev.* **119**, 8506–8554 (2019).
- Peerless, B., Schmidt, A., Franzke, Y. J. & Dehnen, S.  $\phi$ -Aromaticity in prismatic  $[\text{Bi}_6]^{3-}$  clusters. *Nat. Chem.* <https://doi.org/10.1038/s41557-022-01099-5> (2022).
- Mayer, K., Weßing, J., Fässler, T. F. & Fischer, R. A. Intermetallic clusters: molecules and solids in a dialogue. *Angew. Chem. Int. Ed.* **57**, 14372–14393 (2018).
- Wilson, R. J., Weinert, B. & Dehnen, S. Recent developments in Zintl cluster chemistry. *Dalt. Trans.* **47**, 14861–14869 (2018).
- Rienmüller, J. et al. Reactive solubilization of heterometallic clusters by treatment of  $(\text{TrBi}_3)^{2-}$  anions (Tr = Ga, In, Tl) with  $[\text{Mn}\{\text{N}(\text{SiMe}_3)_2\}_2]$ . *Angew. Chem. Int. Ed.* **61**, e202210683 (2022).
- Townrow, O. P. E., Chung, C., Macgregor, S. A., Weller, A. S. & Goicoechea, J. M. A neutral heteroatomic zintl cluster for the catalytic hydrogenation of cyclic alkenes. *J. Am. Chem. Soc.* **142**, 18330–18335 (2020).
- Sevov, S. C. & Goicoechea, J. M. Chemistry of deltahedral Zintl ions. *Organometallics* **25**, 5678–5692 (2006).
- van IJzendoorn, B. et al. A Zintl cluster for transition metal-free catalysis: C=O bond reductions. *J. Am. Chem. Soc.* **144**, 21213–21223 (2022).
- Townrow, O. P. E., Duckett, S. B., Weller, A. S. & Goicoechea, J. M. Zintl cluster supported low coordinate Rh(I) centers for catalytic H/D exchange between  $\text{H}_2$  and  $\text{D}_2$ . *Chem. Sci.* **13**, 7626–7633 (2022).
- Wang, Y. et al. Site selective  $\text{CO}_2$  reduction over highly dispersed Ru-SnO<sub>x</sub> sites derived from  $[\text{Ru}@\text{Sn}_9]^{6-}$  Zintl cluster. *ACS Catal.* **10**, 7808–7819 (2020).
- Poitiers, N. E., Giarrana, L., Huch, V., Zimmer, M. & Scheschkewitz, D. Exohedral functionalization: vs. core expansion of siliconoids with Group 9 metals: Catalytic activity in alkene isomerization. *Chem. Sci.* **11**, 7782–7788 (2020).
- Morgan, H. W. T., Shu, C. C., Sun, Z. M. & McGrady, J. E. Missing link in the growth of lead-based Zintl clusters: isolation of the dimeric plumbaspherene  $[\text{Cu}_4\text{Pb}_{22}]^{4-}$ . *J. Am. Chem. Soc.* **144**, 8007–8017 (2022).
- Wang, J. Q., Stegmaier, S., Wahl, B. & Fässler, T. F. Step-by-step synthesis of the endohedral stannaspherene  $[\text{Ir}@\text{Sn}_{12}]^{3-}$  via the capped cluster anion  $[\text{Sn}_9\text{Ir}(\text{cod})]^{3-}$ . *Chem. Eur. J.* **16**, 1793–1798 (2010).
- Kesani, B. et al. Cluster growth and fragmentation in the highly fluxional platinum derivatives of  $\text{Sn}_9^{4-}$ : Synthesis, characterization, and solution dynamics of  $\text{Pt}_2@\text{Sn}_{17}^{4-}$  and  $\text{Pt}@\text{Sn}_9\text{H}^{3-}$ . *J. Am. Chem. Soc.* **129**, 4567–4574 (2007).
- Li, Z., Ouyang, D. & Xu, L.  $[\text{Bi}_7\text{M}_3(\text{CO})_3]^{2-}$  (M = Co, Rh): a new archetype of 10-vertex deltahedral hybrids by the unprecedented polycyclic  $\eta^5$ -coordination addition of  $\text{Bi}_7^{3-}$  and trimetallic fragments. *Chem. Commun.* **55**, 6783–6786 (2019).
- Li, Z., Liu, C., Wu, J., Lin, Z. & Xu, L.  $[(\eta^3\text{-Bi}_3)_2(\text{IrCO})^6(\mu^4\text{-Bi})_3]^{3-}$ : A new archetype of a 15-vertex deltahedral hybrid from  $\text{BiX}^{3-}$  coordination aggregation of cationic  $[\text{IrCO}]^+$  units. *Dalt. Trans.* **48**, 12013–12017 (2019).
- Chen, S. et al. Aggregation of polybismuthide anions in a single compound using  $^+\text{Rh-CO}$  units: heterometallic cluster ions  $[\text{Rh}@\text{Bi}_{10}(\text{RhCO})_6]^{3-}$  and  $[\text{Rh}@\text{Bi}_9(\text{RhCO})_5]^{3-}$ . *Inorg. Chem.* **59**, 10628–10633 (2020).
- Whitmire, K. H., Churchill, M. R. & Fettinger, J. C. Synthesis and crystal structure of  $[\text{Et}_4\text{N}]_2[\text{Bi}_4\text{Fe}_4(\text{CO})_{13}]$ : discovery of a hybrid Zintl-metal carbonyl cluster. *J. Am. Chem. Soc.* **4**, 1056–1057 (1985).
- Goicoechea, J. M., Hull, M. W. & Sevov, S. C. Heteroatomic deltahedral clusters: synthesis and structures of closo- $[\text{Bi}_3\text{Ni}_4(\text{CO})_6]^{3-}$ , closo- $[\text{Bi}_4\text{Ni}_4(\text{CO})_6]^{2-}$ , the open cluster  $[\text{Bi}_3\text{Ni}_6(\text{CO})_9]^{3-}$ , and the intermetallic closo- $[\text{Ni}_x@\text{Bi}_6\text{Ni}_6(\text{CO})_8]^{4-}$ . *J. Am. Chem. Soc.* **129**, 7885–7893 (2007).
- Goicoechea, J. M., Hull, M. W. & Sevov, S. C. Heteroatomic deltahedral clusters: synthesis and structures. *J. Am. Chem. Soc.* **4**, 7885–7893 (2007).
- Qiao, L., Chen, D., Zhu, J., Muñoz-Castro, A. & Sun, Z. M.  $[\text{Bi}_6\text{Mo}_3(\text{CO})_9]^{4-}$ : a multiple local  $\sigma$ -aromatic cluster containing a distorted  $\text{Bi}_6$  triangular prism. *Chem. Commun.* **57**, 3656–3659 (2021).
- Perla, L. G. & Sevov, S. C.  $[\text{Bi}_{12}\text{Ni}_7(\text{CO})_4]^{4-}$ : aggregation of intermetallic clusters by their thermal deligation and oxidation. *Inorg. Chem.* **54**, 8401–8405 (2015).
- Xu, L., Ugrinov, A. & Sevov, S. C. Stabilization of ozone-like  $[\text{Bi}_3]^{3-}$  in the heteroatomic closo-clusters  $[\text{Bi}_3\text{Cr}_2(\text{CO})_6]^{3-}$  and  $[\text{Bi}_3\text{Mo}_2(\text{CO})_6]^{3-}$ . *J. Am. Chem. Soc.* **2**, 4091–4092 (2001).
- Eulenstein, A. R. et al. Substantial  $\pi$ -aromaticity in the anionic heavy-metal cluster  $[\text{Th}@\text{Bi}_{12}]^{4-}$ . *Nat. Chem.* **13**, 149–155 (2021).
- Eulenstein, A. R. et al. Stabilizing a metalloid  $\{\text{Zn}_{12}\}$  unit within a polymetallic environment in  $[\text{K}_2\text{Zn}_{20}\text{Bi}_6]^{6-}$ . *Nat. Commun.* **11**, 5122 (2020).
- Weinert, B., Eulenstein, A. R., Ababei, R. & Dehnen, S. Formation of  $[\text{Bi}_{11}]^{3-}$ , a homoatomic, polycyclic bismuth polyanion, by pyridine-assisted decomposition of  $[\text{GaBi}_3]^{2-}$ . *Angew. Chem. Int. Ed.* **53**, 4704–4708 (2014).
- Weinert, B., Müller, F., Harms, K., Clérac, R. & Dehnen, S. Origin and location of electrons and protons during the formation of intermetallic clusters  $[\text{Sm}@\text{Ga}_{3-x}\text{H}_{3-2x}\text{Bi}_{10+x}]^{3-}$  (x = 0, 1). *Angew. Chem. Int. Ed.* **53**, 11979–11983 (2014).
- Xu, L. & Sevov, S. C. Heteroatomic deltahedral clusters of main-group elements: synthesis and structure of the Zintl ions  $[\text{In}_4\text{Bi}_5]^{3-}$ ,  $[\text{InBi}_3]^{2-}$ , and  $[\text{GaBi}_3]^{2-}$ . *Inorg. Chem.* **39**, 5383–5389 (2000).
- Kaas, M. & Korber, N. Cyclic tribismuthide as a piano stool complex ligand—synthesis and crystal structure of  $(\eta^3\text{-Bi}_3)\text{M}(\text{CO})_3^{3-}$  (M = Cr, Mo). *Z. Anorg. Allg. Chem.* **645**, 146–148 (2019).
- TURBOMOLE pre-version 7.7.2022 (University of Karlsruhe and Forschungszentrum Karlsruhe, 1989–2007, and TURBOMOLE, since 2007, accessed 13 February 2022); <http://www.turbomole.com> (2022).
- Tao, J., Perdew, J. P., Staroverov, V. N. & Scuseria, G. E. Climbing the density functional ladder: nonempirical meta-generalized gradient approximation designed for molecules and solids. *Phys. Rev. Lett.* **91**, 146401 (2003).
- Weigend, F. & Baldes, A. Segmented contracted basis sets for one- and two-component Dirac-Fock effective core potentials. *J. Chem. Phys.* **133**, 174102 (2010).
- Metz, B., Stoll, H. & Dolg, M. Small-core multiconfiguration-Dirac-Hartree-Fock-adjusted pseudopotentials for post-d main group elements: application to PbH and PbO. *J. Chem. Phys.* **113**, 2563–2569 (2000).
- Schäfer, A., Klamm, A., Sattel, D., Lohrenz, J. C. W. & Eckert, F. COSMO implementation in TURBOMOLE: extension of an efficient quantum chemical code towards liquid systems. *Phys. Chem. Chem. Phys.* **2**, 2187–2193 (2000).
- Xu, L., Bobev, S., El-Bahraoui, J. & Sevov, S. C. A naked diatomic molecule of bismuth,  $[\text{Bi}_2]^{2-}$ , with a short Bi-Bi bond: Synthesis and structure. *J. Am. Chem. Soc.* **122**, 1838–1839 (2000).
- Osar, A. & Corbett, J. I. Polybismuth anions. synthesis and crystal structure of a salt of the tetrabismuthide(2-) ion,  $\text{Bi}_4^{2-}$ . A basis for the interpretation of the structure of some complex intermetallic phases. *Inorg. Chem.* **85**, 2482–2487 (1977).
- Kocak, F. S. et al. Surprising acid/base and ion-sequestration chemistry of  $\text{Sn}_9^{4-}$ :  $\text{HSn}_9^{3-}$ ,  $\text{Ni}@\text{HSn}_9^{3-}$ , and the  $\text{Sn}_9^{3-}$  ion revisited. *J. Am. Chem. Soc.* **134**, 9733–9740 (2012).
- Hull, M. W. & Sevov, S. C. Functionalization of nine-atom deltahedral Zintl ions with organic substituents: detailed studies of the reactions. *J. Am. Chem. Soc.* **131**, 9026–9037 (2009).
- Sheldrick, G. M. SHELXT-integrated space-group and crystal-structure determination. *Acta Crystallogr. A Struct. Chem.* **71**, 3–8 (2015).
- Dolomanov, O. V., Bourhis, L. J., Gildea, R. J., Howard, J. A. K. & Puschmann, H. OLEX2: a complete structure solution, refinement and analysis program. *J. Appl. Crystallogr.* **42**, 339–341 (2009).

54. Diamond—Crystal and Molecular Structure Visualization, Crystal Impact—Dr. H. Putz & Dr. K. Brandenburg GbR, Kreuzherrenstr. 102, 53227 Bonn, Germany. <http://www.crystalimpact.com/diamond> (2023).
55. Boys, S. F. Construction of some molecular orbitals to be approximately invariant for changes from one molecule to another. *Rev. Mod. Phys.* **32**, 296–299 (1960).

### Acknowledgements

The authors thank the German Research Foundation (Deutsche Forschungsgemeinschaft, DFG) for financial support. The work was co-funded by the European Union (ERC, BiCMat, 101054577). Views and opinions expressed are however those of the author(s) only and do not necessarily reflect those of the European Union or the European Research Council. Neither the European Union nor the granting authority can be held responsible for them. We acknowledge fruitful discussion with Dr. Lukas Guggolz and Andreas Schmidt.

### Author contributions

S.D. and K.B. designed the experiments. K.B. performed the experimental, analytical, and computational work. S.D., K.B., and B. P. interpreted the data and discussed the findings. All authors co-wrote the manuscript.

### Funding

Open Access funding enabled and organized by Projekt DEAL.

### Competing interests

The authors declare no competing interests.

### Additional information

**Supplementary information** The online version contains supplementary material available at <https://doi.org/10.1038/s42004-023-00905-6>.

**Correspondence** and requests for materials should be addressed to Stefanie Dehnen.

**Peer review information** *Communications Chemistry* thanks Tiankai Chen and the other, anonymous, reviewers for their contribution to the peer review of this work.

**Reprints and permission information** is available at <http://www.nature.com/reprints>

**Publisher's note** Springer Nature remains neutral with regard to jurisdictional claims in published maps and institutional affiliations.



**Open Access** This article is licensed under a Creative Commons Attribution 4.0 International License, which permits use, sharing, adaptation, distribution and reproduction in any medium or format, as long as you give appropriate credit to the original author(s) and the source, provide a link to the Creative Commons licence, and indicate if changes were made. The images or other third party material in this article are included in the article's Creative Commons licence, unless indicated otherwise in a credit line to the material. If material is not included in the article's Creative Commons licence and your intended use is not permitted by statutory regulation or exceeds the permitted use, you will need to obtain permission directly from the copyright holder. To view a copy of this licence, visit <http://creativecommons.org/licenses/by/4.0/>.

© The Author(s) 2023